Decadal variability in 20th Century ocean acidification in the California Current Ecosystem

Emily B. Osborne[1,2*], Robert C. Thunell[3,†], Nicolas Gruber[4], Richard A. Feely[5] & Claudia R. Benitez-Nelson[3]

[1]Ocean Acidification Program, National Oceanic and Atmospheric Administration, Silver Spring, Maryland, USA. [2]Cooperative Program for the Advancement of Earth System Science, University Corporation for Atmospheric Research, Boulder, Colorado, USA. [3]School of the Earth, Ocean and Environment, University of South Carolina, Columbia, South Carolina, USA. [4]Environmental Physics, Institute of Biogeochemistry and Pollutant Dynamics, ETH Zürich, Zürich, Switzerland. [5]Pacific Marine Environmental Laboratory, National Oceanic and Atmospheric Administration, Seattle, Washington, USA.

†Deceased July 30, 2018

*Corresponding author: Correspondence in reference to this manuscript can be sent to Emily B. Osborne (emily.osborne@noaa.gov)

Oceanic uptake of CO_2 can mitigate climate change, but also results in global ocean acidification. Ocean acidification-related changes to the marine carbonate system can disturb ecosystems and hinder calcification by some organisms. Here, we use the calcification response of planktonic foraminifera as a tool to reconstruct the progression of ocean acidification in the California Current Ecosystem through the 20th Century. Measurements of nearly 2,000 fossil foraminifera shell weights and areas preserved in a marine sediment core showed a 20% reduction in calcification by a surface-dwelling foraminifera species. Using modern calibrations, this response translates to an estimated 35% reduction in carbonate ion concentration, a biologically important chemical component of the carbonate system. Assuming other aspects of the carbonate system, this represents a 0.21 decline in pH, exceeding the estimated global average decline by more than a factor of two. Our proxy record also shows considerable variability that is significantly correlated with Pacific Decadal Oscillation and decadal-scale changes in upwelling strength, a relationship

that until now has been obscured by the relatively short observational record. This modulation suggests that climatic variations will play an important role in amplifying or alleviating the anthropogenic signal and progression of ocean acidification in this region.

Since the beginning the industrial era, atmospheric CO_2 levels have risen from 280 ppm to more than 400 ppm; an unprecedented concentration over the past 800,000 years (Lüthi et al., 2008). The oceans have absorbed approximately 27% of this anthropogenic CO_2, which has caused an estimated 0.1 reduction in global mean surface-ocean pH; the phenomenon known as ocean acidification (OA) (Orr et al., 2005; Feely et al., 2004, 2009; Khatiwala et al., 2013; Le Quéré et al., 2015; Gruber et al., 2019). Field studies of some of the ocean's major calcium carbonate producing organisms, often indicate a negative calcification response declining [CO_3^{2-}] (e.g., Fabry et al., 2008; Ries et al., 2009; De'ath et al., 2009; Meier et al., 2014; Moy et al., 2009; de Moel et al., 2009; Bednarsek et al., 2017; Riebesell et al., 2016), although in some instances calcification remains unaffected or is even enhanced (e.g., Rivero-Calle et al., 2015; Iglesias-Rodriguez et al., 2008).

Research suggests that OA is becoming particularly acute in coastal upwelling regions, such as the CCE, due to their low buffering capacity and the natural upwelling processes that bring CO_2-rich intermediate waters to the ocean surface (e.g. Orr et al., 2005; Feely et al., 2008, 2016, 2018; Hauri et al., 2009; Gruber et al., 2012; Turi et al 2016). Models indicates a considerable decline in [CO_3^{2-}] in the CCE and a shoaling of the saturation horizons for each of the $CaCO_3$ mineral polymorphs (calcite Ω_{cal} and aragonite Ω_{arg}) since the onset of industrial period, reducing the volume of the surface-

ocean favorable for calcification (Gruber et al., 2012; Hauri et al., 2013; Turi et al., 2016). Modern sampling has identified malformed and dissolved aragonite-secreting pteropods during periods of strong upwelling when the saturation horizon comes very close to or even intersects with the sea surface (Bednarsek et al., 2014, 2017; Feely et al., 2008).

Initial surveys of the global ocean marine carbonate system only began in the late 1970's, well after anthropogenic carbon began altering the marine carbonate system (GEOSECS; Takahashi et al., 1982). Specifically within the CEE, *in situ* sustained observations of carbonate system variables are limited to the last decade (California Cooperative Oceanic Fisheries Investigations or CalCOFI; 2009-present). While these observational records are critically important to our understanding of ocean chemistry, they do not provide a sufficiently long historical record of this phenomenon. The lack of long-term OA records limits our ability to place recent observations into the context of past change and hinders an assessment of natural decadal climate oscillation impacts on the marine carbonate system. Model simulations can close the knowledge gap but without constraints from *in situ* and/or proxy measurements, their validity remains unknown, especially with regard to their skill in capturing variability. Here, we provide the first century-long nearly annually resolved OA proxy record for the central region of the CCE and investigate 20th century trends and decadal-scale processes at play.

Carbonate chemistry and calcification

A number of studies have demonstrated that the carbonate chemistry of seawater strongly influences the calcification of planktonic foraminifera, leaving a distinct imprint on the *thickness* of their shells. This has permitted researchers to use shell weight as a

proxy for past surface-ocean [CO_3^{2-}]. However shell weight also inherently reflects shell size, which is controlled dominantly by ambient temperature and perhaps other variables (Mashiotta et al., 1997; Spero et al., 1997; Bijma et al., 1999; Barker & Elderfield, 2002; see Methods for extended discussion). Here, we use a relatively new shell weight technique (Marshall et al., 2013) that effectively size-normalizes individual shell weights (Methods), called area normalized shell weight (ANSW) that can be used to quantitatively assess shell thickness and by extension [CO_3^{2-}]. We apply this technique to the ubiquitously occurring surface-mixed layer species, *Globigerina bulloides*, to reconstruct ambient-[CO_3^{2-}] over the past 100 years, building upon a proof of concept for this species and method by Osborne et al. 2016 (Methods). Previous research on *G. bulloides* has suggested that the calcification and growth of this species might be also influenced by ambient temperature, nutrient concentration or "optimal growth conditions" (Aldridge et al., 2012, Beer et al., 2010, de Villers 2003). The Osborne et al. (2016) study examined sediment trap collections and a sediment core record of *G. bulloides* shell weight, area and diameter data to closely evaluated these relationships and provided robust evidence that ANSW is directly controlled by ambient [CO_3^{2-}], rather than temperature or nutrient concentration (R^2 0.80, Standard Error of the Estimate ±16 μmol kg^{-1}) (See Methods for discussion; Extended Data Figure 1).

Here, the ANSW of nearly 2,000 individual *G. bulloides* shells were measured using 58 sediment samples from a 0.48-meter long box-core collected in an anoxic region of the Santa Barbara Basin (SBB; 34˚14'N, 120˚02'W; 580 m water depth: Extended Data Figure 2). A radioisotope-based age model was developed for this 100-year laminated and unbioturbated sediment core (1898 to 2006 ± 6 years) (See Methods;

104 Osborne et al., 2016). Down core ANSW and shell diameter measurements indicate that
105 on average *G. bulloides* produced 20% thinner and 7% larger shells, respectively, by the
106 close of the 20th century relative to those from 1900 (Extended Data Figure 3 and 4). To
107 assess if *G. bulloides* shell thickness and by extension [CO_3^{2-}] has declined significantly
108 over the core record, we examine decadal population averages of ANSW (**Figure 1**).
109 These averages indicate that shell thicknesses from the 1990-2000 populations are indeed
110 significantly thinner than the 1900-1910 populations (95% confidence). The decline in
111 ANSW is further apparent in scanning electron micrographs of shell wall thicknesses of
112 *G. bulloides* from the top and bottom of the sediment core (**Figure 1**). There is an
113 apparent increase in the rate of change that occurs roughly between the first half and the
114 second half of the core. This change in slope appears to be associated with a greater
115 frequency of low [CO_3^{2-}] events occurring in the more recent portion of the record,
116 thereby reducing the overall average [CO_3^{2-}] during the later interval. Several notable
117 [CO_3^{2-}] events recorded in our proxy record coincide with low [CO_3^{2-}] outputs in SBB
118 model simulations (Turi et al., 2016) and occur in association with the timing of several
119 strong El Niño events (1982-83, 1987-88, 1997-97).
120 By applying the ANSW-[CO_3^{2-}] relationship presented by Osborne et al. (2016)
121 to our downcore ANSW measurements, we estimate that surface ocean [CO_3^{2-}] in the
122 SBB decreased by 35% representing a net change of approximately 98 μmol kg^{-1} ± 16 in
123 [CO_3^{2-}] over the 20th century (from 271 ± 16 μmol kg^{-1} in 1895 to 173 ± 16 μmol kg^{-1} in
124 2000; **Figure 2**). Recent *in situ* surface ocean [CO_3^{2-}] measurements from the SBB by
125 NOAA's WCOA data (2011-2013) and by CalCOFI (2009-2015) and are in excellent
126 agreement with the forward projected trend of our estimated [CO_3^{2-}] values even though

these datasets do not temporally overlap. The time-series slopes, used to determine a decadal rate of change, recorded by our proxy reconstruction (-9.992 μmol $kg^{-1}dec^{-1}$) and the integrated CalCOFI and WCOA data (-10.716 μmol $kg^{-1}dec^{-1}$) are within error of one another. An additional comparison to the HOT dataset from the North Pacific (Dore et al., 2009) also shows a similar long-term decline (-6.616 μmol $kg^{-1}dec^{-1}$), albeit with significantly higher [CO_3^{2-}] values and a lesser rate of decline, illustrating the inherently low [CO_3^{2-}] conditions in the CCE. Hindcast model simulations for the CCE indicate a long-term trend (-5.431, -5.397, -4.949 μmol $kg^{-1}dec^{-1}$ at 0, 30 and 50 m, respectively) that is also in agreement with our proxy record, however, simulations indicate overall lower rate of change and [CO_3^{2-}] values relative to our ANSW based estimates, which is likely a result of negative biases that exist in the employed model configuration (Hauri et al., 2013, Turi et al., 2016, see Methods).

Because the relative concentrations of the dissolved inorganic carbon species in seawater (dissolved inorganic carbon (DIC); CO_2, HCO_3^-, CO_3^{2-}) co-vary in a predictable nature, so do the variables of the marine carbonate system (DIC, Total Alkalinity (TA), pH, pCO_2). We use an empirical salinity-TA relationship derived for the CCE coastal zone and sea surface salinity measurements from the Scripps Pier (1916-present) time-series to estimate TA for our record (Fassbender et al., 2016). For the period when no salinity observations exist (1895-1915) a best-fit linear regression is used to estimate salinity values. Realizing this approach incorporates a great deal of uncertainly, particularly when applied to the paleo record, we use a combination of our down core proxy-[CO_3^{2-}] and a salinity-TA estimates to roughly characterize the full carbonate system to report how the most commonly used measure of OA, pH, has

150 evolved over the last century in order to compare to other published results (see
151 Methods). These estimates indicate that [H^+] of seawater has increased by 80%,
152 translating into a 0.21 unit decline in pH that exceeds the global average of 0.1 units by
153 more than a factor of two (Caldeira & Wickett, 2003). We do not report error on this
154 estimate as there are a number of assumptions made for these calculations and a reported
155 value would likely underestimate uncertainty. However, our calculated decadal rate of pH
156 decline for this region over the last century (-0.021 dec^{-1}) is consistent with the rate of pH
157 decline modeled for the entire CCE (-0.020 dec^{-1}; 1979-2012; Turi et al., 2016), and
158 larger scale observations for the North Pacific: -0.017 dec^{-1} from 1991-2006 (Byrne et al.,
159 2010) and -0.019 dec^{-1} from 1988-2014 (Bates et al., 2014; Dore et al., 2009). Our results
160 are also consistent with large declines in pH resulting from strong upwelling as depicted
161 by regional model simulations for the central region of the CCE (Gruber et al., 2012; Turi
162 et al., 2016).

163 **Disentangling drivers of ocean acidification**

164 The surface ocean carbonate system in our study region is influenced by a
165 combination of exposure to atmospheric CO_2, local introduction of waters with low
166 [CO_3^{2-}] via shifts in upwelling and surface circulation, and local changes in productivity.
167 To evaluate the dominating mechanism(s) driving the 20th century changes in the upper
168 water column carbonate system, we use the down core foraminiferal stable isotopic
169 records as tools to track carbon source and water column structure.

170 The $\delta^{13}C$ record of *G. bulloides* and two other foraminifera species
171 (*Neogloboquadrina incompta and Neogloboquadrina dutertrei*) sampled from the core
172 show significant (R^2 = 0.46, 0.36, and 0.34, respectively $p < 0.005$) long-term declines in

173 $\delta^{13}C$ (**Figure 3**). The observed increase in the surface ocean inventory of anthropogenic
174 carbon sourced from ^{12}C-enriched fossil fuel causes an overall decline in the $\delta^{13}C$ of
175 seawater; a globally observed phenomenon termed the The Suess Effect (Keeling et al.,
176 1979, Gruber et al., 1999). Additionally, variability in local productivity and upwelling of
177 DIC and ^{12}C-rich intermediate- and deep-water (from respiration and remineralization)
178 could also influence surface ocean, and by extension foraminiferal, $\delta^{13}C$. The observed
179 long-term decline in $\delta^{13}C$ is consistent with an increase in ^{13}C-depleted anthropogenic
180 CO_2 stemming primarily from the uptake from the atmosphere, strengthened upwelling, a
181 decline in productivity, or a combination of these processes.
182 A $[CO_3^{2-}]$ effect has been observed on stable isotope signatures recorded by
183 foraminifera, whereby elevated $[CO_3^{2-}]$ results in relatively lower $\delta^{13}C$ (Spero et al.,
184 1997). Considering the $[CO_3^{2-}]$ effect on foraminiferal $\delta^{13}C$, we estimate that based on
185 the culture derived relationship of Spero et al. (1997) for 13-chambered *G. bulloides* and
186 the change in carbonate ion concentration estimated by our proxy record, that $\delta^{13}C$ would
187 increase by 0.94‰ from the years 1895 to 2000, rather than the measured decrease of -
188 0.72‰. This modeled change in the *opposite* direction is consistent with other similar
189 studies and suggests that the magnitude of foraminiferal $\delta^{13}C$ depletion may actually be
190 much larger when the $[CO_3^{2-}]$ effect is removed (Black et al., 2011).
191 Considering the influence of upwelling on our $\delta^{13}C$ record, a majority of model
192 evidence for the CCE suggests that coastal upwelling will be enhanced in coastal Eastern
193 Boundary Upwelling Systems (EBUS) due to climate induced strengthening of along-
194 shore winds that drive Ekman-upwelling (e.g., Sydeman et al., 2014). However, historical
195 observations from the CalCOFI time-series (1950-present) in the SBB report stratifying

196 conditions over the latter half of the 20th century associated with warming sea surface
197 temperatures, deepening of the thermocline depth, and declining zooplankton biomass
198 (Roemmich and McGowan, 1995; McGowan et al., 2003; Di Lorenzo et al., 2005). Using
199 the $\Delta\delta^{18}$O-water column structure proxy, we compare δ^{18}O signatures recorded by the
200 surface mixed layer species, *G. bulloides*, to the thermocline to deep-dwelling
201 foraminifera species, *N. incompta*, to infer the depth of the thermocline and stability of
202 the mixed layer (Pak and Kennett, 2002). The observed increase in $\Delta\delta^{18}$O represents and
203 increasing offset in depth habitat and therefore a decline in upwelling strength, providing
204 further evidence of 20th century CCE stratification, which would hypothetically result in
205 an *increase* in δ^{13}C over our record rather than the observed decrease (**Figure 3**).
206 Shifts in dinoflagellate cyst assemblages in the SBB also suggest a reduction in upwelling
207 and shed light on an overall reduction in seasonal primary productivity throughout the
208 20th century (Bringue et al., 2014). While this reduction in productivity is consistent with
209 the sign of our δ^{13}C record, we argue that the magnitude of productivity change is not
210 great enough to persistently drive the observed δ^{13}C record. Rather, productivity in the
211 CCE and other EBUS may be a synergistic factor and important on shorter time-scales.
212 Collectively, our records indicate that the increasing surface ocean inventory of
213 anthropogenic CO_2 is the dominant long-term control on δ^{13}C and by extension [CO_3^{2-}]
214 recorded in our proxy record. This is supported by the fact that owing to a relatively
215 robust scaling between the ^{13}C Suess effect and the increase in anthropogenic CO_2 of
216 about -0.017 permil (μmol kg^{-1})$^{-1}$ (Sonnerup and Quay, 2012), the long-term decrease in
217 δ^{13}C of about 0.72‰ over the 1895 to 2000 period implies an increase in anthropogenic
218 CO_2 of about 42 μmol kg^{-1}. This is a bit smaller than the expected increase of about 50

219 μmol kg^{-1} over this period, but supporting our conclusion of a dominant contribution of
220 the uptake of anthropogenic CO_2 to our reconstructed decrease in the [CO_3^{2-}].

221 **Decadal-scale variability**

222 While we attribute the long-term reduction in [CO_3^{2-}] largely to air-sea exchange
223 of anthropogenic CO_2, considerable variability exists around the declining trend. In order
224 to best visualize this variability, we de-trended the [CO_3^{2-}] record, revealing decadal and
225 sub-decadal scale oscillations that are significantly correlated with the PDO index (Hare
226 et al., 1996) ($R^2 = 0.53$, $p<0.005$; Extended Data Figure 5) (**Figure 4**). During positive
227 (warm) phases of PDO the carbonate system shifts to a higher [CO_3^{2-}] state, while
228 negative (cool) phases of PDO coincide with overall lower [CO_3^{2-}] values (**Figure 4a**).
229 PDO is associated with decadal time-scale changes in the strength of the Aleutian Low,
230 resulting in basin-wide temperature, pressure and wind stress anomalies in the Pacific
231 Ocean (Mantua and Hare, 2002). Within the CCE, the positive (warm) phase of PDO
232 coincides with weaker Aleutian Low winds, resulting in decreased coastal upwelling,
233 warmer sea surface temperatures and reduced productivity. Conversely, the negative
234 (cold) phase of PDO produces the opposite set of conditions.

235 Since coastal upwelling controls the amount of low pH, CO_2-rich waters that
236 reach the surface and PDO regulates the strength of upwelling, we hypothesize that this
237 mechanism alters the surface carbonate system on decadal time-scales. El Niño and La
238 Niña events, typically lasting 6-18 months, produce similar anomalies and have already
239 been observed in association with sustained changes in coastal upwelling and acidity of
240 surface waters off the continental shelf of California (Nam et al., 2011).

We use our de-trended stable isotopic records ($\delta^{13}C$ and $\Delta\delta^{18}O$) to evaluate variability occurring independently of the long-term trend. We find that residual trends in $\delta^{13}C$ and $\Delta\delta^{18}O$ clearly co-vary with PDO; positive phases are marked by a higher $\Delta\delta^{18}O$ and $\delta^{13}C$ signatures, which represent decreased upwelling/increased stratification and warmer temperatures (**Figure 4**). We also use the individual calcification response to assess upwelling variability based on a similar foraminiferal depth habitat premise as the $\Delta\delta^{18}O$ proxy. During periods of strengthened upwelling less intra-sample variability is expected for a given *G. bulloides* population since a shoaled thermocline would tighten the suitable habitable depth range for this species, above the thermocline to sea surface. The opposite would be true for stratified conditions. Using sample population standard error as a measure of intra-sample variability, a greater spread in individual ANSW is indeed associated with intervals of positive PDO marked by weaker upwelling relative to negative PDO when stronger upwelling occurs ($R^2 = 0.55$, $p<0.005$, **Figure 5** and Extended Figure 5). These proxy records together corroborate that as upwelling weakens in the CCE during positive PDO, higher [CO_3^{2-}] levels occur while during negative phases of PDO, strengthened upwelling produces persistently lower [CO_3^{2-}] conditions.

Implications for future ocean acidification

Our OA reconstruction indicates a significant long-term 35% decline in [CO_3^{2-}] recorded for the central CCE over the 20th century as a result of increasing concentrations of anthropogenic CO_2 in seawater. Our OA record reveals considerable variability around the long-term trend, which we find to be significantly correlated with decadal-scale changes in upwelling strength associated with the PDO. This implies that over decadal time-scales positive/negative phases of PDO coincide with an overall elevated/reduced

264 [CO_3^{2-}] state as a result of shifts in upwelling strength. The relationship between PDO
265 and OA means that the anthropogenic acidification signal will be both amplified and
266 alleviated in response to decadal shifts in the PDO phase, suggesting that that future
267 progression of OA will be significantly modulated by large-scale climate modes. While
268 projections of [CO_3^{2-}] are important for understanding how the system may progress in
269 the future, our past record indicates [CO_3^{2-}] will not decline linearly and that by climatic
270 forcing will be important in the coming century.
271

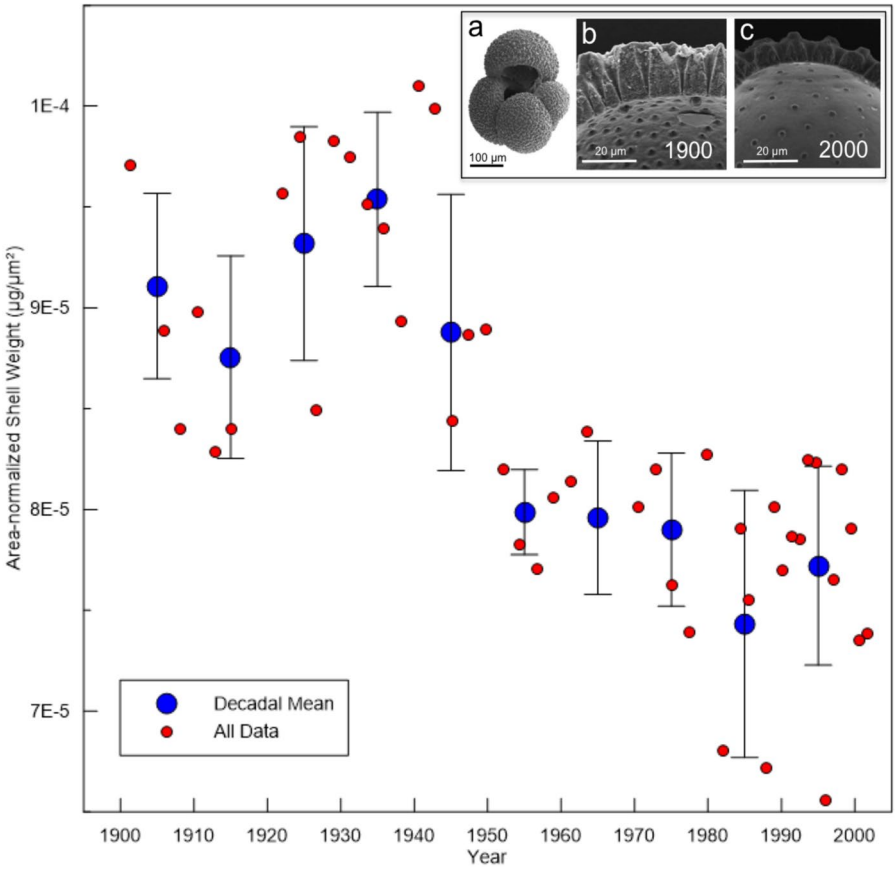

272

273 **Figure 1**. **Decadal population mean area-normalized shell weight plotted with 95%**
274 **confidence intervals.** Red circles show the sample averages for the 58 sediment slices
275 examined in this study. Decadal time-slice populations (blue circles) of mean *G.*
276 *bulloides* ANSW show a significant offset in shell thicknesses measured in 1900-1910
277 and 1990-2000. SEM images show (a) a typical *G. bulloides* specimen from the SBB and

shell wall cross-sections of similarly sized shells from the (b) upper- and (c) lower-most samples of the box-core clearly illustrating the difference in shell wall thickness over the past century.

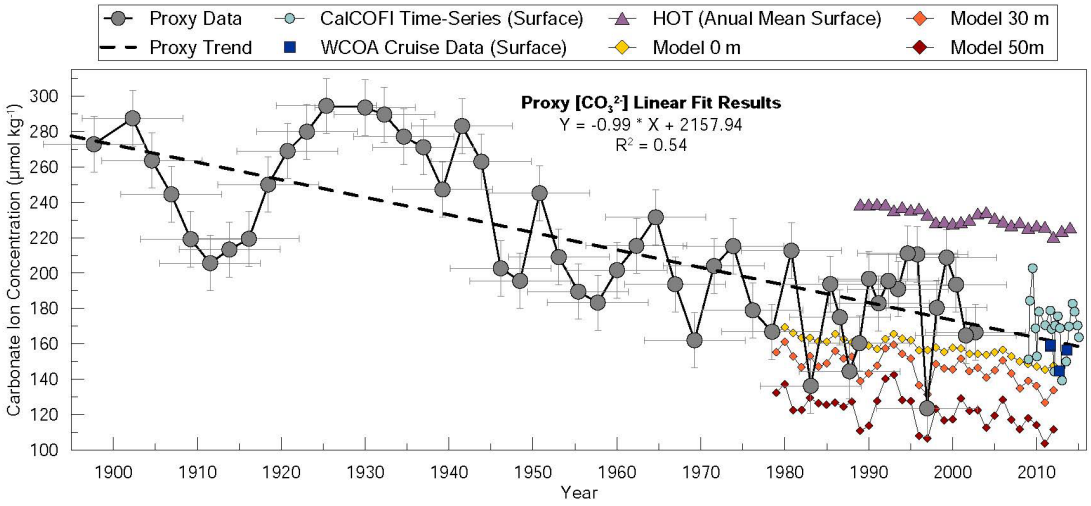

Figure 2. 20th Century proxy [CO_3^{2-}] record based on *G. bulloides* area-normalized shell weight (1895-2000). Horizontal errors represent age uncertainty (±6 years) and vertical errors (±15.63 µmol kg^{-1}) represent the standard error of the estimate associated with the calibration relationship (Osborne et al., 2016). Proxy data are compared to model simulations (1979-2012; Turi et al., 2016) and *in situ* measurements from the Santa Barbara Basin (Feely et al., 2016) and HOT data from the North Pacific (Dore et al., 2009). The average modern [CO_3^{2-}] is 164 µmol kg^{-1} and temperatures is 15°C based on 2010-2015 *in situ* data.

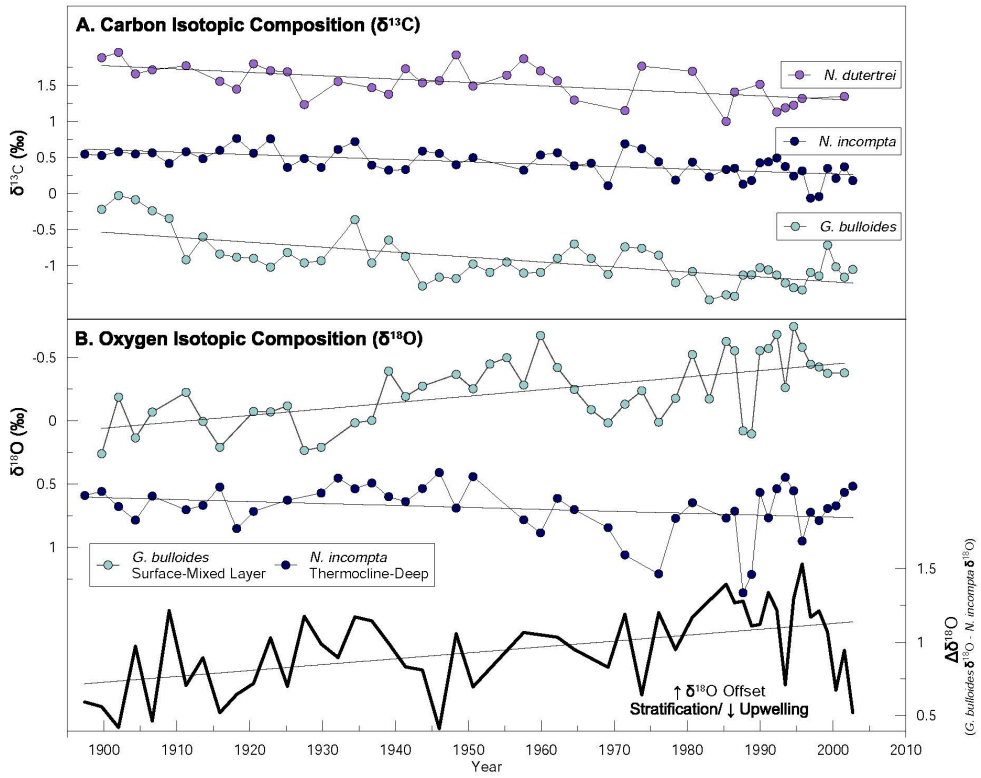

Figure 3. Stable isotope tracers of influential processes. A. $\delta^{13}C$ record of three planktonic foraminifera species, *G. bulloides. N. incompta and N. dutertrei* (R^2 0.46, 0.36, and 0.34, respectively $p < 0.005$) showing a long-term decline consistent with an increasing anthropogenic CO_2 inventory in the surface ocean. B. $\delta^{18}O$ records of *G. bulloides* (surface-mixed layer dwelling species) and *N. incompta* (thermocline-deep dwelling species) that are used to trace the relative depth habitats and as a proxy for changes in the depth of the thermocline and related thickness and stability of the mixed layer (Pak and Kennett, 2002).

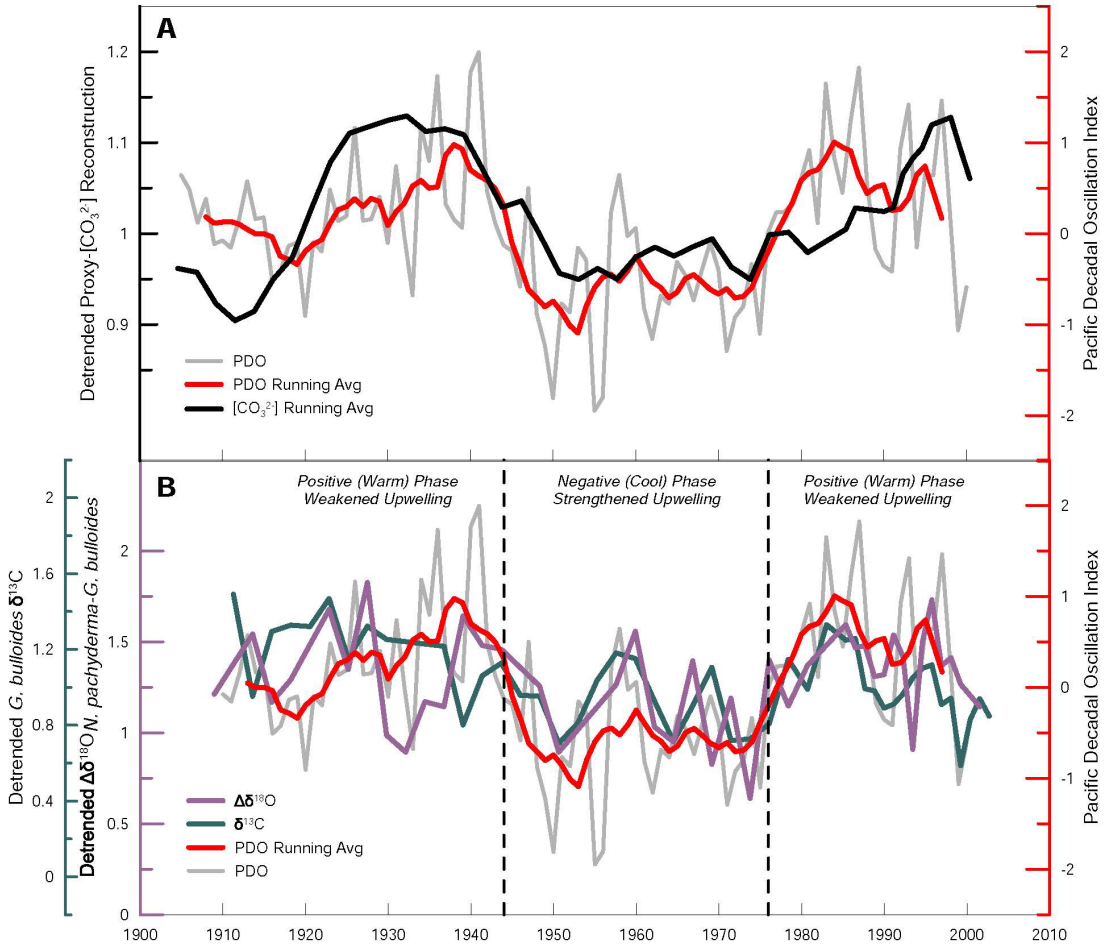

Figure 4. **Linking upwelling strength, Pacific Decadal Oscillation and carbonate system state.** A. The $[CO_3^{2-}]$ record shown with the long-term anthropogenically-driven decline removed (detrended) plotted with the Pacific Decadal Oscillation (PDO) index (Hare et al., 1996). An apparent correlation between high/low $[CO_3^{2-}]$ and positive/negative PDO phases. Both data sets are shown as 5-year running means. B. The detrended $\Delta\delta^{18}O_{(N.\ incompta\text{-}G.\ bulloides)}$ and *G. bulloides* $\delta^{13}C$ again to highlight the natural variability not associated with anthropogenic ocean acidification plotted again with the PDO index indicating a relationship between weakened/strengthened upwelling and positive/negative PDO phase.

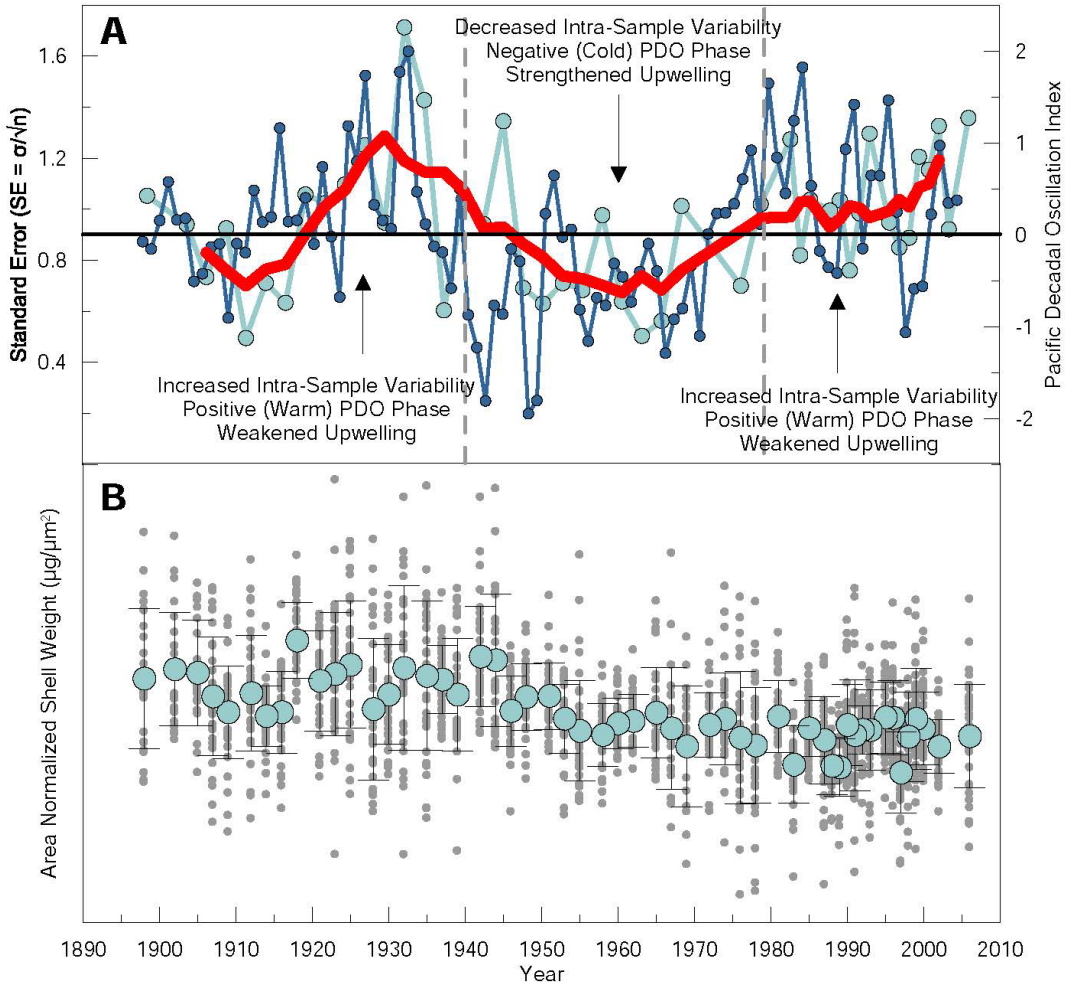

Figure 5. Using Individuals to Trace Habitat Depth and Upwelling Strength. A. Time-series showing the sample ANSW standard error plotted with the Pacific Decadal Oscillation Index. These time-series show increased variability associated with positive (warm) PDO phases that are marked by weakened upwelling strength. B. Individual ANSW measurements (gray circles) plotted with sample average ANSW (blue circle) and associated sample standard error bars.

References

1. Aldridge, D., Beer, C.J., Purdie, D.A. Calcification in the planktonic foraminifera Globigerina bulloides linked to phosphate concentrations in surface waters of the North Atlantic Ocean. Biogeosciences 9, 1725-1739 (2012).
2. Beer, C.J., Schiebel, R., Wilson, P.A. Testing planktic foraminiferal shell weight as a surface water [CO32-] proxy using plankton net samples. Geology 38, 103-106 (2010).
3. Barker, S., and H. Elderfield. Foraminiferal Calcification Response to Glacial-Interglacial Changes in Atmospheric CO_2, *Science* 297, 833-836 (2002).

4. Bednaršek, N., R.A. Feely, J.C.P. Reum, W. Peterson, J. Menkel, S.R. Alin, and B. Hales. Limacina helicina shell dissolution as an indicator of declining habitat suitability due to ocean acidification in the California Current Ecosystem. *Proc. Roy. Soc. Lond. B*, *281* (2014).
5. Bednaršek, N., T. Klinger, C.J. Harvey, S. Weisberg, R.M. McCabe, R.A. Feely, J. Newton, and N. Tolimieri. New ocean, new needs: Application of pteropod shell dissolution as a biological indicator for marine resource management. *Ecol. Indic.*, *76*, 240–244 (2017).
6. Bijma, J., H.J. Spero, and D.W. Lea. Reassessing foraminiferal stable isotope geochemistry: Impact of the oceanic carbonate systems (experimental results). Pp. 489–512 in Use of Proxies in Paleoceanography: Examples from the South Atlantic. G. Fisher and G. Wefer, eds., Springer-Verlag, New York, NY (1999).
7. Black, D., R.C. Thunell, K. Wejnert, and Y. Astor. Carbon isotope composition of Caribbean Sea surface waters: Response to the uptake of anthropogenic CO_2, *Geophys. Res. Lett*. 38 (2011).
8. Byrne RH, Mecking S, Feely R a and Liu X. Direct observations of basin-wide acidification of the North Pacific Ocean, *Geophys. Res. Lett*. 37 1–5 (2010).
9. Caldeira, K. & Wickett, M. E. Anthropogenic carbon and ocean pH. Nature 425, 365 (2003).
10. de Moel, H., G. M. Ganssen, F. J. C. Peeters, S. J. A. Jung, D. Kroon, G. J. A. Brummer, and R. E. Zeebe. Planktic foraminiferal shell thinning in the Arabian Sea due to anthropogenic ocean acidification? *Biogeosciences*, 6, 1917–1925 (2009).
11. De Villiers, S. Optimum growth conditions as opposed to calcite saturation as a control on the calcification rate and shell-weight of marine foraminifera. Mar Biol, 10.1007/s00227-00003-01183-00228.Dee DP et al 2011 The ERA-Interim reanalysis: configuration and performance of the data assimilation system Q. J. R. Meteorol. Soc. 137 553–97 (2003).
12. Di Lorenzo E, Miller AJ, SchneiderNand McWilliams JC. The warming of the California current system: dynamics and ecosystem implications, *J. Phys. Oceanogr*. 35 336–62 (2005).
13. De'ath, G., J. M. Lough, K. E. Fabricius. Declining coral calcification on the Great Barrier Reef, *Science* 342 (6158) 599, doi: 10.1126/science.1165283.
14. Dore, J.E., R. Lukas, D.W. Sadler, M.J. Church and D.M. Karl (2009) Physical and biogeochemical modulation of ocean acidification in the central North Pacific. Proceedings of the National Academy of Sciences USA, 106, 12235-12240 (2009).
15. Feely, R. A., Sabine, C. L., Lee, K., Berelson, W., Kleypas, J., Fabry, V. J., Millero, F. J. Impact of Anthropogenic CO_2 on the $CaCO_3$ System in the Oceans. *Science* 305, 362-366 (2004).
16. Feely, R. A., C. L. Sabine, J. M. Hernandez-Ayon, D. Ianson, and B. Hales. Evidence for Upwelling of Corrosive 'Acidified' Water onto the Continental Shelf. *Science* 320 (5882), 1490–92 (2008).
17. Feely, R.A., et al., Chemical and biological impacts of ocean acidification along the west coast of North America, Estuarine, Coastal and Shelf Science (2016).
18. Feely, R.A., R.R. Okazaki, W.-J. Cai, N. Bednaršek, S.R. Alin, R.H. Byrne, and A. Fassbender. The combined effects of acidification and hypoxia on pH and

aragonite saturation in the coastal waters of the Californian Current Ecosystem and the northern Gulf of Mexico. *Cont. Shelf Res.*, *152*, 50–60 (2018).
19. Ferguson, J. E., K. R. Johnson, G. Santos, L. Mayer, A. Tripati. Investigating δ13C and Δ14C within Mytilus californianus shells as proxies of upwelling intensity, *Geochem. Geophys. Geosys.,* 14 (6) 1856-1865 (2013).
20. Fabry, V., Seibel, B., Feely, R., and Orr, J. Impacts of ocean acidification on marine fauna and ecosystem processes, ICES Journal of Marine Science 65, 414-432 (2008).
21. Fassbender, A. J., S. R. Alin, R. A. Feely, A. J. Sutton, J. A. Newton, R. H. Byrne. Estimating total alkalinity in the Washington State Coastal Zone: Complexities and surprising utility for ocean acidification research, *Estuaries and Coasts* (2016).
22. Gruber, N., C. D. Keeling, R. B. Bacastow, P. R. Guenther, T. J. Lueker, M. Wahlen, H. A. J. Meijer, W. G. Mook, and T. F. Stocker. Spatiotemporal patterns of carbon-13 in the global surface oceans and the oceanic Suess effect, *Glob. Biogeochem. Cycles*, 13(2), 307–335 (1999).
23. Gruber, N. and others. The Ocean Sink for Anthropogenic CO_2 from 1994 to 2007, *Science* 363, 1193-1199 (2019).
24. Gruber, N., C. Hauri, Z. Lachkar, D. Loher, T.L. Frölicher, and G. Plattner. Rapid Progression of Ocean Acidification in the California Current System, *Science* 337, 220-223 (2012).
25. Hare, S. R. Low frequency climate variability and salmon production. Ph.D. Dissertation. Univ. of Washington, Seattle, WA, 306 pp (1996).
26. Hauri, C., Gruber, N., Plattner, G., Alin, S., Feely, R. A., Hales, B., Wheeler, P. A. Ocean acidification in the California Current System, *Oceanography* 22, 60-71 (2009).
27. Hauri, C., N. Gruber, A. M. P. McDonnell, M. Vogt. The intensity duration and severity of low aragonite saturation state events on the California continental shelf *Geophysical Research Letters* 40, 3424-3429 (2013).
28. Keeling, C. D. The Suess effect: ^{13}Carbon-^{14}Carbon interrelations, *Environ. Int.*, *2*(4–6), (1979).
29. Khatiwala, S., Tanhua, T., Mikaloff Fletcher, S., Gerber, M., Doney, S. C., Graven, H. D., Gruber, N., McKinley, G. A., Murata, A., Ríos, A. F., and Sabine, C. L. Global ocean storage of anthropogenic carbon, *Biogeosciences*, 10, 2169–2191, (2013).
30. Le Quéré, C., and others. Global Carbon Budget 2015, *Earth Syst. Sci. Data*, 7, 349-396, (2015).
31. Lüthi et al. High-Resolution Carbon Dioxide Concentration Record 650,000-800,000 years before Present. *Nature* 453, 379-382, 2008.
32. McGowan, J., S. Bograd, R. J. Lynn, and A. J. Miller. The biological response to the 1977 regime shift in the California Current. Deep-Sea Res., 50, 2567–2582 (2003).
33. Mantua, N. J. and Hare, S. R. The Pacific decadal oscillation, *J. Oceanogr*. 58 35–44, (2002).
34. Marshall, B.J., R. Thunell, M. Hennehan, Y.Astor, and K. Wejnert. Planktonic foraminiferal area density as a proxy for carbonate ion concentration: A calibration study using the Cariaco Basin ocean time series, *Paleoceanography* 28, 1-14,

(2013).
35. Meier, K. J. S., L. Beaufort, S. Heussner, and P. Ziveri. The role of ocean acidification in *Emiliania huxleyi* coccolith thinning in the Mediterranean Sea, *Biogeosciences* 11, 2857-2869 (2014).
36. Moy, A.D., W.R. Howard, S.G.Bray, and T.W. Trull. Reduced calcification in modern Southern Ocean planktonic foraminifera, *Nature Geoscience* 2, 276–280 (2009).
37. Nam, S., H-J Kim, and U. Send. Amplification of hypoxic and acidic events by La Nina conditions on the continental shelf off California, *Geophys. Res. Lett.*, 38, (2011).
38. Orr, James C., V. J. Fabry, O. Aumont, L. Bopp, S.C. Doney, R.A. Feely, A. Gnanadesikan, et al. Anthropogenic Ocean Acidification over the Twenty-First Century and Its Impact on Calcifying Organisms. *Nature* 437 (7059), 681–86 (2005).
39. Osborne, E. B., R. C. Thunell, B. J. Marshall, J. A. Holm, E. J. Tappa, C. Benitez-Nelson, W.-J. Cai, and B. Chen. Calcification of the planktonic foraminifera *Globigerina bulloides* and carbonate ion concentration: Results from the Santa Barbara Basin, Paleoceanography, 3 (2016).
40. Pak, D. K., and J. P. Kennett. A Foraminiferal Isotopic Proxy for Upper Water Mass Stratification, *The Journal of Foraminiferal Research* 32 (3), 319–27 (2002).
41. Ries, J. B., A. L. Cohen, and D. C. McCorkle. Marine calcifiers exhibit mixed responses to CO2-induced ocean acidification, Geology, 37(12), 1131–1134, (2009).
42. Roemmich, D. and J. McGowan. Climatic warming and the decline of zooplankton in the California Current. *Science*, 267, 1324–1326 (1995).
43. Sonnerup, R. E., and P. D. Quay. 13 C constraints on ocean carbon cycle models, *Global Biogeochem. Cycles*, *26*(2), 1–16 (2012).
44. Spero, H.J., J. Bijma, D.W. Lea, and B.E. Bemis. Effect of seawater carbonate concentration on foraminiferal carbon and oxygen isotopes, *Nature* 390(6659), 497–500 (1997).
45. Sydeman, W. J., M. Garcia-Reyes, D. S. Schoeman, R. R. Rykaczewski, S. A. Thompson, B.A. Black and S. J. Bograd. Climate Change and wind intensification in coastal upwelling ecosystems, *Science* 345, 77-80 (2014).
46. Takahashi, T., R.T. Williams, and D.L. Bos. Carbonate chemistry. Pp. 77–83 in GEOSECS Pacific Expedition, vol. 3, Hydrographic Data 1973–1974. W.S. Broecker, D.S. Spencer, and H. Craig, eds, National Science Foundation, Washington, DC (1982).
47. Turi, G., Z. Lachkar, N. Gruber, M. Munnich. Climatic modulation of recent trends in ocean acidification in the California Current System, *Environ. Res. Lett.* 11 (2016).

Acknowledgements

We dedicate this manuscript to co-author Robert Thunell, a wonderful colleague, friend and mentor, who lost his battle to cancer on July 30, 2018. This research was supported in part by a National Science Foundation grant to Robert Thunell (1631977) and the Johanna M. Resig Fellowship granted to Emily Osborne by the Cushman Foundation.

Richard Feely's portion of this work was supported by the NOAA Ocean Acidification Program (PMEL Contribution number 4546). Nicolas Gruber would also like to acknowledge the support of ETH Zürich and of the Swiss National Foundation through the XEBUS project. We would like to thank Dr. David Burdige from Old Dominion University for collecting the box-core used in this study. Thank you to Eric Tappa for his assistance with IRMS analyses and sediment trap recovery and deployments in the Santa Barbara Basin. Thank you to Dr. Natalie Umling whose thoughtful review and scientific discourse greatly improved this manuscript. And finally, thank you to our reviewers whose comments greatly improved and shaped the final form of this manuscript.

Author Contributions

E.B.O. and R.C.T conceived the study and wrote the initial draft of the paper. E.B.O. designed and performed the analyses and has led the revision of the paper. N.G. and R.A.F. provided model and *in situ* data and contributed significantly to the discussion and interpretation of the results and writing of the paper. C.B.N conducted radiochemistry analyses producing an age model for the core and contributed to the interpretation and writing of the paper.

Data Availability Statement

The authors declare that the data supporting the findings of this study are available within the article. New data generated as a part of this study have been made publicly available via the PANGAEA Data Archiving portal (PDI-21505). Additional data related to this study are available from the corresponding author upon request. Publicly available data used in this study are described below. Carbonate chemistry measurements made within the SBB were collected seasonally by the California Cooperative Oceanic Fisheries Investigations time-series (CalCOFI; http://calcofi.org/) and during several NOAA West Coast Ocean Acidification Cruises (WCOA; https://www.nodc.noaa.gov/ocads/oceans/Coastal/WCOA.html). Observational data from the Hawaii Ocean Time-series program (HOT; http://hahana.soest.hawaii.edu/hot/) are also included. Shore Station Data (Salinity) for carbonate system calculations.

Extended Data

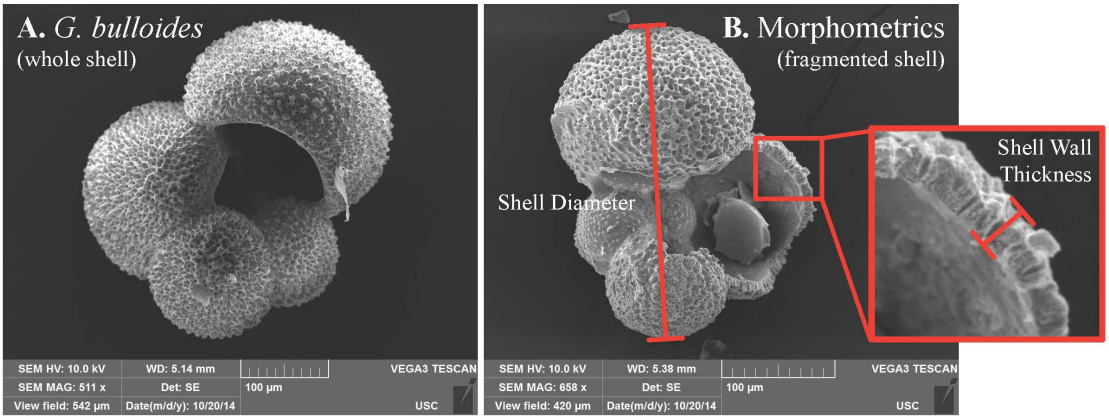

Extended Data Figure 1. A. Scanning Electron Microscope images of the study species, *G. bulloides*. B. *G. bulloides* shell with its final chamber broken showing a cross-sectional view of the shell wall, the key morphometric used in this study to estimate $[CO_3^{2-}]$. Shell wall thickness is indirectly estimated by measuring area normalized shell weight (ANSW: shell weight (µg) / 2-D surface area (μm^2).

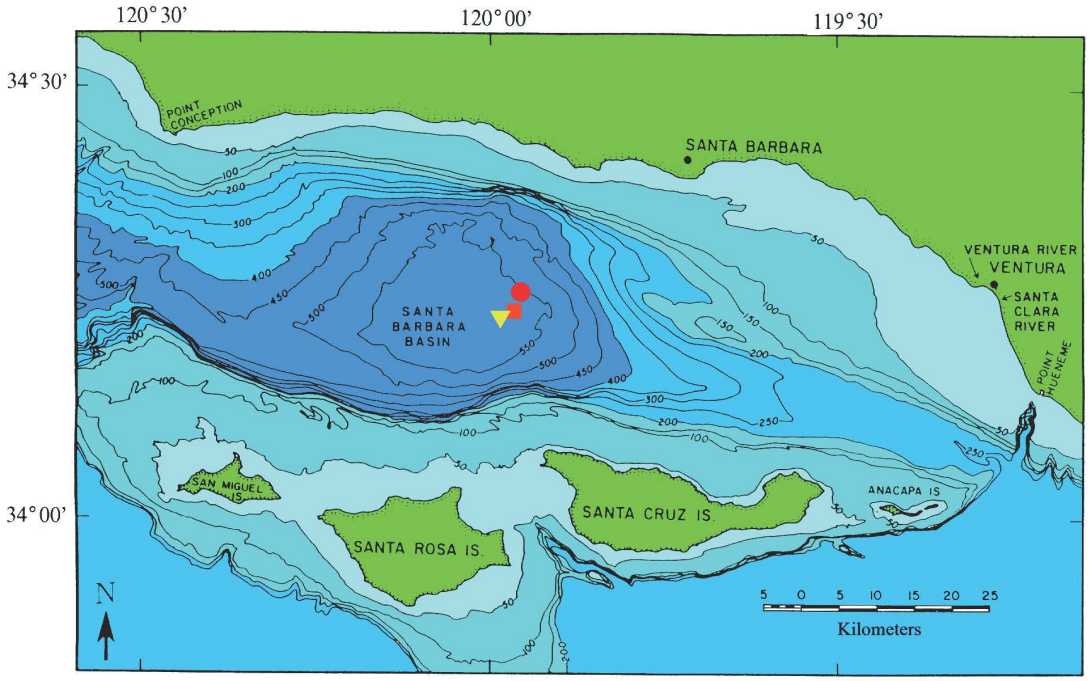

Extended Data Figure 2. Bathymetric map of the Santa Barbara Basin. The location of the box-core (red circle) used for the down-core reconstruction as well as the sediment trap (yellow triangle) and hydrographic sampling location (Plumes and Blooms Project Station 4; orange square) used in the calibration portion of the study (Osborne et al., 2016).

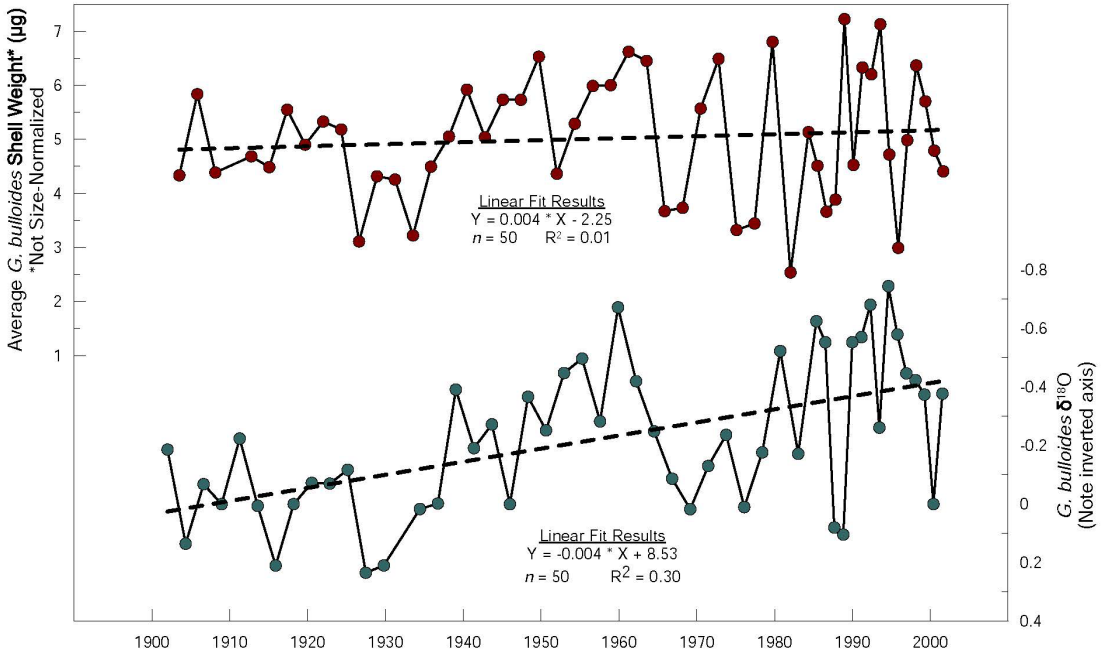

Extended Data Figure 3. Down core trends in G. bulloides weight (not size-normalized) and $\delta^{18}O$. The increasing shell weight over the down core record coincides with a decline in $\delta^{18}O$ (note inverted axis), which represents an increase in temperature. This comparison provides a visualization of the importance of using size-normalized shell weights to estimate changes in calcification and shell thickness. Results from this study show that while overall shell weight and shell size are increasing as a result of warming temperatures, shell thickness is declining as a result of reduced [CO_3^{2-}].

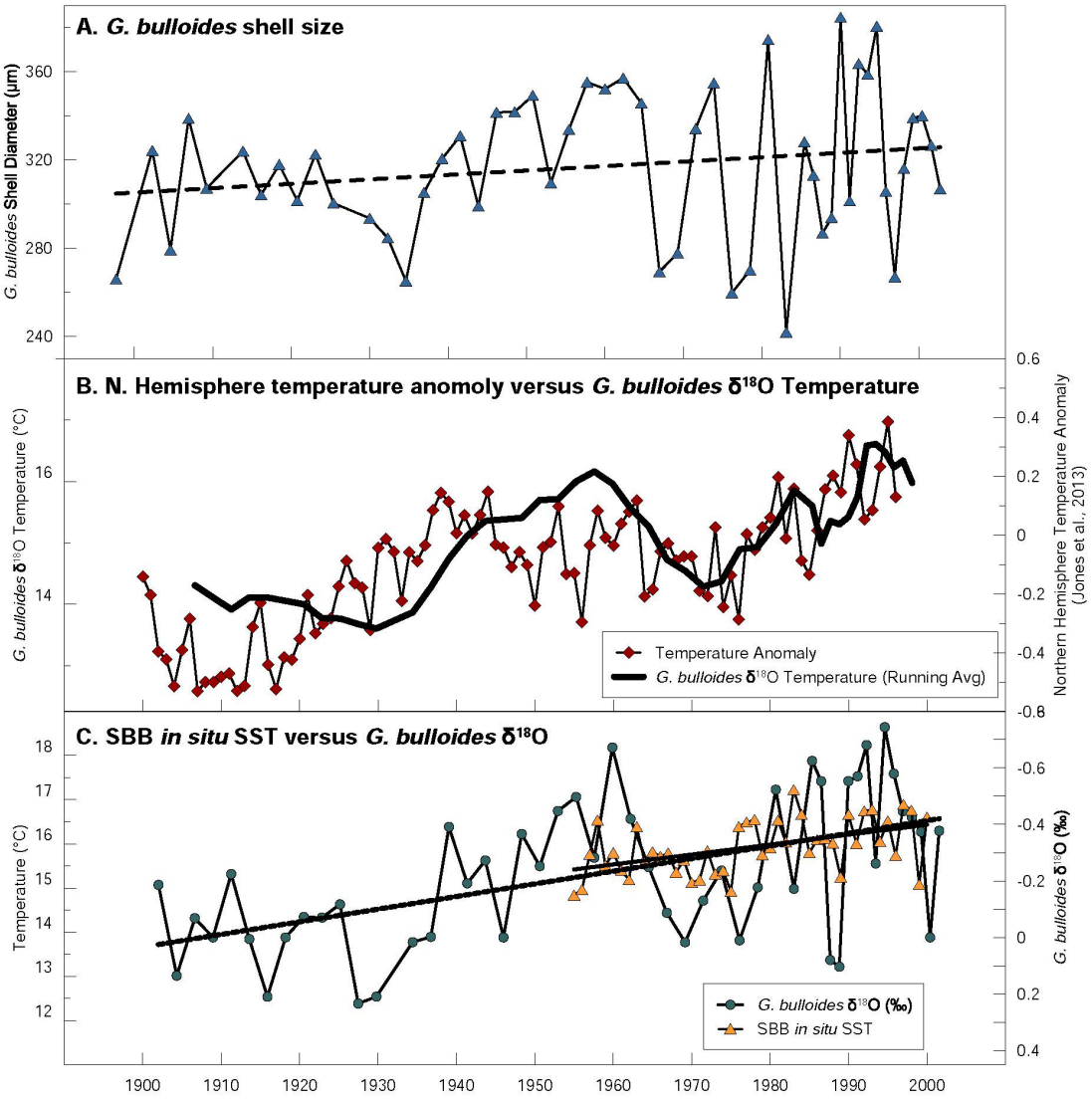

Extended Data Figure 4. The long-term shift in *G. bulloides* shell diameter increases in concert with warming sea surface temperatures. B. We compare the relative changes that are recorded *G. bulloides* $\delta^{18}O$ to a Northern Hemisphere Temperature anomaly for the 1900-2000 period and see a good agreement between temperature trends recorded in these records (Jones et al., 2013). C. We also compared *G. bulloides* δ18O to in situ sea surface temperature (SST) measurements made in the Santa Barbara Basin (SBB; 1955-Present; Shore Stations Program) and see an excellent agreements between sea surface temperature and the $\delta^{18}O$ recorded in our *G. bulloides* shells.

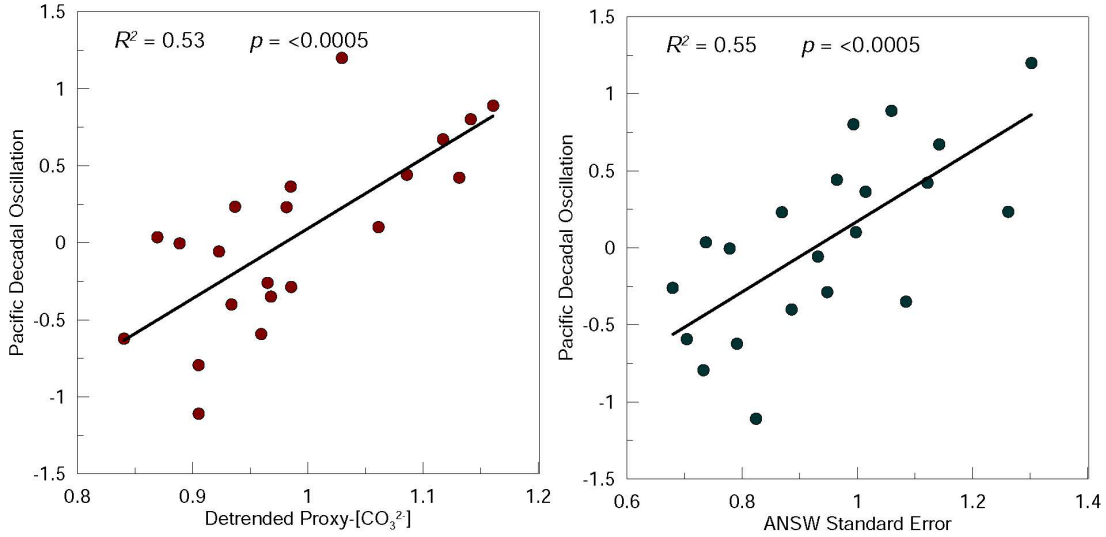

Extended Data Figure 5. Time-series correlations between Pacific Decadal Oscillation Index and the detrended proxy-[CO_3^{2-}] and ANSW sample standard error. Corresponding values were compared at 5-year time steps due to difference in time resolution across records. An independent t-test was conducted to compare both detrended proxy-[CO_3^{2-}] and area-normalized shell weight standard area (a measure of sample variability) to the Pacific Decadal Oscillation Index. Highly significant correlation coefficients exist between PDO and the respective variables $p<0.005$) and the results of a paired t-tests for both records are highly significant ($p<0.005$), further confirming significance of the relationships.

Methods

Area Normalized Shell Weight While several shell weight size-normalization techniques used to estimate foraminiferal calcification and shell thickness exist, we chose to use the area density method, also known as area-normalizing shell weight (ANSW) that uses individual rather than bulk population measurements (Marshall et al., 2013). This method is currently the most effective size-normalization technique (compared to measure-based weights and sieve-based weights) that best constrains shell thickness (Osborne et al., 2016; Marshall et al., 2013). The inability to effectively size-normalize shell weight measurements results in datasets that are not only influenced by CO_3^{2-} but also by temperature, as temperature results in larger and heavier shells but has no effect on shell thickness. See Osborne et al. (2016) for in depth discussion and review of previously published results for this species.

We aimed to pick 40 individual *G. bulloides* shells from the >150 μm size-fraction of each sediment sample for ANSW analyses. On average 35 individuals are included in each ANSW data point, (maximum 40 and minimum 17 individuals), representing a total of 1,870 analyzed shells included in this dataset. Individual *G. bulloides* shells with abnormally formed shells or that had visible clay and/or organic material were excluded from our analyses as these characteristics could effect weight and area measurements. The presence of an encrusted cryptic morphospecies of *G. bulloides* has been documented in the Santa Barbara Channel (Sautter and Thunell., 1991, Darling et al., 2000; Bemis et al., 2002). Further investigation indicated that the less abundant and cool water loving "encrusted" morphospecies calcifies and fractionates stable carbon and oxygen isotopes differently than the more abundant "normal" morphospecies (Bemis et al., 2002; Osborne et al., 2016). Due to the offset in ANSW and the intention to use these *G. bulloides* shells for later stable isotope analyses, morphometric measurements collected during ANSW processing are also used to identify and remove encrusted individuals from our sample populations (Osborne et al., 2016; Marshall et al., 2015). The species-specific ANSW response of the normal *Globigerina bulloides* morphospecies to ambient [CO_3^{2-}] has been constrained using individuals collected in the Santa Barbara Basin (SBB) by a sediment trap time-series (Equation 2). Stable isotope results from this 3.5-year sediment-trap analysis indicate that on average *G. bulloides* calcify in the 40 m depth range, although seasonal variability in depth habit does occur in association with upwelling.

While there can still be a considerable amount of variability within a single sediment sample, statistical analyses by Osborne et al. (2016) demonstrate the asymptotic nature of the % error as a function of numbers of individuals used in an ANSW measurement. These results suggest that a pool of 30-40 individuals represents a high degree of confidence when using a mean area density value to represent the population mean. Each shell is individually weighed in a copper weigh boat using a high precision microbalance (Mettler Toledo XP2U; ±0.43 μg) in an environmentally controlled weigh room. Next, each individual is photographed positioned umbilical side up using a binocular microscope (Zeiss Stemi 2000-C) fitted with a camera (Point Grey Research Flea3 1394b). The microscopic imaging program (Orbicule Macnification 2.0) was used to analyze shells photos for length (Feret diameter) and the 2-D surface area or silhouette. The Macnification 2.0 program uses the RGB images to calculate a region of interest and generates an outline of the shell image, which is then used to estimate a pixel 2-D area. Pixel measurements are converted to lengths (μm) and areas (μm^2) by calibrating an image of a 1 mm microscale

taken at the same magnification and working distance as shell photos. Individual shell weights were then divided by their corresponding areas and a mean ANSW value was calculated for each sample population. These ANSW values were then applied to the calibration relation relationship (equation 1) presented by Osborne et al. (2016) to estimate $[CO_3^{2-}]$.

$$[CO_3^{2-}] = (ANSW - 4.19*10^{-5})/ 1.92*10^{-7} \quad \text{(Equation 1)}$$

Age Model Development Approximately 2 grams from each sample were freeze dried and used for radioisotope measurements. Wet weights, recorded prior to freeze drying, and dry weights were used to estimate sample porosity and correct for compaction. Freeze dried sediments were ground, loaded into counting vials and sealed with epoxy for 3 weeks prior to counting. Each sample was measured (3-5 days) for ^{210}Pb, ^{214}Pb and ^{137}Cs via gamma decay counting using a high purity germanium well detector [*Moore,* 1984].

The excess ^{210}Pb ($^{210}Pb_{ex}$), reflective of atmospheric deposition rather than supported ^{210}Pb ($^{210}Pb_{supp}$) from the decay of ^{226}Ra, was determined by subtracting the activity of ^{214}Pb (assumed to be in secular equilibrium with $^{210}Pb_{supp}$; mean 3.7 dpm/g) from the activity of ^{210}Pb. The exponential decay of $^{210}Pb_{ex}$ observed in the core sediments (Figure 3) used to determine ages for the core using a combination of Constant Initial Concentration (CIC) and Constant Rate of ^{210}Pb Supply (CRS) models. An offset of approximately ±1 year was observed between models. Using these age constraints an average sedimentation rate of 0.43 cm y^{-1}; and an average mass accumulation rate of 5.84 g cm^2 y^{-1} was determined for the core. The sedimentation rate determined from the $^{210}Pb_{ex}$ is relatively uniform over the entire 0.5 m core and is also in good agreement with previously determined radioisotope chronologies for the SBB (Koide et al., 1972; Krishnaswami et al., 1973, Bruland et al., 1974). The increase in ^{137}Cs activity at 19 cm (Figure 3) is used as an independent age marker horizon for the year 1964 and represents the peak in radioactive fallout from atmospheric nuclear bomb testing (Carter and Moghissi, 1977; Ritchie and McHenry, 1989). The depth of the ^{137}Cs spike was shallower than expected using both the CRS and CIC models when assuming a 2012 collection year as the core top age. We therefore conclude that the upper several centimeters of sediments were not preserved when this box-core was collected. As such, we applied a 6-year age correction, which is also used as the age error estimate, anchored the 19 cm ^{137}Cs spike to a depositional year of 1964. These age constraints indicate that the 0.5 meter core extends back to ~1895 and the uppermost sediments contained in the core represent the year ~2006.

CCE Marine Carbonate System Model Simulation The model-based estimates of the progression of the carbonate ion concentration in the Santa Barbara Basin stem from the simulations described in detail by Turi et al. (2016). Annual mean data were extracted from the model at the four nearest gridpoints to the location of the core from various depths, i.e., 0 m, 30m, and 50 m. The model is based on the UCLA-ETH version of the Regional Oceanic Modeling System (Shchepetkin and McWilliams 2005), and includes a nitrogen-based nutrient-phytoplankton zooplankton-detritus model (Gruber et al 2006) that was extended with a carbon module (Gruber et al 2012, Hauri et al 2013). The CalCS model setup employed here has a horizontal resolution of 5 km and 34 levels in the vertical and

spans the entire U.S. coast from about 30° N to 50° N and extends more than 1300 km into the Pacific. The hindcast simulation (1979-2012) was forced at the surface with fluxes of heat and freshwater from ECMWF' s ERA-Interim reanalysis (Dee et al 2011). The boundary conditions at the lateral boundaries of the model consisted of a combination of climatological fields based on observations and time-varying anomaly fields derived from a global hindcast simulation with theNCAR CCSM3 model (Graven et al 2012). The evaluation of the model simulated pH and saturation state with respect to aragonite, Ω_{arag} with observations revealed that the model is capturing the large-scale offshore and depth gradients very well, but that it has a slight positive bias in the nearshore regions north of Point Conception (Hauri et al., 2013). Owing to the lack of in situ measurements from the Santa Barbara Basin, no assessment could be undertaken in this part of the CalCS, but also the comparison with the time series records from Santa Monica Bay (Leinweber and Gruber, 2013) suggest a slight overestimation of the modeled pH and Ω_{arag} in the upper ocean.

Stable Isotope Measurements At least 100 µg (30-40 individuals) of *G. bulloides* used for ANSW analyses were pooled to measure the stable oxygen ($\delta^{18}O$) and carbon ($\delta^{13}C$) isotopic composition. Foraminifera were cleaned for 30 minutes in 3% H_2O_2 followed by a brief sonication and acetone rinse prior to analyses. Stable isotope measurements were carried out on an Isoprime isotope ratio mass spectrometer equipped with a carbonate preparation system. The long-term standard reproducibility is 0.07‰ for $\delta^{18}O$ and 0.06‰ for $\delta^{13}C$. Results are reported relative to Vienna Pee Dee Belemnite (V-PDB).

Marine Carbonate System Calculations Carbonate system variables for the historic record were determined using the CO2Sys Program (Version 2.1). Total alkalinity and dissolved inorganic carbon were used as master input variables (Equations 2 & 3) and *in situ* measurements of sea surface temperature and salinity as input conditions when data are available (Shore Stations Program). Sea surface salinity measurements from the Scripps Pier (1916-present) located just south of our study region and sea surface temperature measurements from the SBB (1955-present) were used for our calculations. A comparison of more recent salinity measurements from the SBB and Scripps Pier indicate that salinity values in these two regions are comparable. For the period from 1916-1954 when SST was not measured in the SBB but was measured at Scripps Pier, we use an average offset between the overlapping periods of these datasets (1955-1900) to extrapolate an SST for the SBB. For the period from 1900-1916 when there is no hydrographic data available, we use the time-integrated relationship for temperature and salinity to estimate these parameters.

We solve for our input master variables (total alkalinity and dissolved inorganic carbon) by coupling proxy [CO_3^{2-}] estimates and a salinity-based estimate of total alkalinity (Fassbender et al., 2016). Although this salinity-alkalinity relationship was derived using carbonate system measurements for the coastal Oregon CCE, a complication of CalCOFI data from the SBB yield a relationship that is within error of the published Fassbender et al. (2016) dataset. We also incorporate total boron into our estimate of total alkalinity, which was determined using the R program seacarb (Total Boron Package; Lee et al., 2010). In order to estimate DIC we sum the estimated [CO_3^{2-}] with the derived

$[HCO_3^-]$ and assume that any concentration of $[CO_2]$ is less than 1% of DIC (Zeebe and Wolf-Gladrow, 2001; Equation 3).

$$\text{Total Alkalinity} = [HCO_3^-]+2[CO_3^{2-}]+[B(OH)_4^-] \quad (2)$$

$$\text{Dissolved Inorganic Carbon} = [HCO_3^-]+[CO_3^{2-}] \quad (3)$$

References

48. Bemis, B. E., H. J. Spero, and R. C. Thunell, Using species-specific paleotemperature equations with foraminifera: a case study in the Southern California Bight, *Marine Micropaleo.*, 46, 405-430 (2002).
49. Bruland, K. W., Pb-210 geochronology in the coastal marine environment [Ph.D. dissert.]:La Jolla, Univ. California, San Diego, 106 p. (1974).
50. Carter, M.W. and A.A. Moghissi, Three Decades of Nuclear Testing, *Health Physics.*, 33, 55-71 (1977).
51. Darling, K.F.,Wade, C.M., Steward, I.A., Kroon, D., Dingle, R., Leigh Brown, A.J., Molecular evidence for genetic mixing of Arctic and Antarctic subpolar populations of planktonic foraminifers. *Nature* 405, 43–47 (2000).
52. Fassbender, A.J., S. R. Alin, R.A. Feely, A.J. Sutton, J.A. Newton, and R.H. Byrne, Estimating Total Alkalinity in the Washington State Coastal one: Complexities and Surprising Utility for Ocean Acidification Research. *Estuaries and Coasts* 40(2), 1-15 (2016).
53. Graven H.D, N. Gruber, R. Key, S, Khatiwala and Giraud. Changing controls on oceanic radiocarbon: new insights on shallow-to-deep ocean exchange and anthropogenic CO2 uptake *J. Geophys. Res.* 117 (2012).
54. Gruber N, Frenzel H, Doney SC, Marchesiello P, McWilliams JC, Moisan J R, Oram J J, Plattner G-K and Stolzenbach, Eddy-resolving simulation of plankton ecosystem dynamics in the California current system *Deep-Sea Res. I* 53 1483–516 (2006).
55. Gruber N, Hauri C, Lachkar Z, Loher D, Frölicher T L and Plattner G-K. Rapid progression of ocean acidification in the California current system *Science* 337 220–3 (2012).
56. Hauri C, Gruber N, Vogt M, Doney SC, Feely R A, Lachkar Z, Leinweber A, McDonnell A, MünnichMand Plattner G-K. Spatiotemporal variability and long-term trends of ocean acidification in the California Current System *Biogeosciences* 10 193–216 (2013).
57. Koide, M., A. Soutar, and E. D. Goldberg. Marine geochronology with Pb-210, *Earth and Planetary Sci. Letters*, 14, 422-446 (1972).
58. Krishnaswami, S., D. Lai, S. Amin, and A. Soutar. Geochronological studies in Santa Barbara Basin: Fe-55 as a unique tracer for particulate settling, *Limnology and Oceanography*, 18, 763-770, (1973).
59. Lee, K., T.-W. Kim, R. H. Byrne, Y.-M. Liu. The universal ratio of boron to chlorinity for the North Pacific and North Atlantic Oceans, *Geochimica et Cosmochimia Acta*, 74(6), 1801-1811 (2010).

60. Leinweber A, and Gruber N. Variability and trends of ocean acidification in the Southern California current system: a timeseries from Santa Monica Bay *J. Geophys. Res.* 118 3622–33 (2013).
61. Marshall, B.J., R. Thunell, M. Hennehan, Y.Astor, and K. Wejnert. Planktonic foraminiferal area density as a proxy for carbonate ion concentration: A calibration study using the Cariaco Basin ocean time series, *Paleoceanography* 28, 1-14, (2013).
62. Osborne, E. B., R. C. Thunell, B. J. Marshall, J. A. Holm, E. J. Tappa, C. Benitez-Nelson, W.-J. Cai, and B. Chen. Calcification of the planktonic foraminifera *Globigerina bulloides* and carbonate ion concentration: Results from the Santa Barbara Basin, Paleoceanography, 31, (2016).
63. Ritchie, J. C., and J. R. McHenry. Application of radioactive fallout Cesium-137 for measuring soil erosion and sediment accumulations rates and patterns: A review, *J. Environ. Qual.*, 19, 215-233 (1989).
64. Sautter, L. R., and R.C. Thunell. Seasonal Variability in the $\delta^{18}O$ and $\delta^{13}C$ of planktonic foraminifera from an upwelling environment: Sediment trap results from the San Pedro Basin, Southern California Bight: Paleoceanography, 6(3), 307-334 (1991).
65. Shchepetkin A F and McWilliams JC. The regional oceanic modeling system (ROMS): a split-explicit, free-surface, topography-following-coordinate oceanic model *Ocean Modelling* 9 347–404 (2005).
66. Zeebe, R. E. and D. A. Wolf-Gladrow. CO2 in Seawater: Equilibrium, Kinetics, Isotopes. Elsevier Oceanography Series, 65, pp. 346, Amsterdam (2001).